Stability of Load Lifting by a Quadrotor under Attitude Control Delay

Pedro O. Pereira and Dimos V. Dimarogonas

***Abstract*— We propose a control law for stabilization of a quadrotor-load system, and provide conditions on the control law's gains that guarantee exponential stability of the equilibrium. The system is composed of a load and an unmanned aerial vehicle (UAV) attached to each other by a cable of fixed length, which behaves as a rigid link under tensile forces; and the control input is composed of a three dimensional force requested to the UAV, which the UAV provides with or without delay. Given the proposed control law, we analyze the stability of the equilibrium in two separate parts. In the first, the system is modeled assuming that the UAV provides the requested control input without delay, and we verify that the equilibrium is exponentially stable. In the second part, the UAV is modeled as possessing an attitude inner loop, and we provide a lower bound on the attitude gain for which exponential stability of the equilibrium is preserved. An integral action term is also included in the control law, which compensates for battery drainage or model mismatches, such as an unknown load mass. We present experiments for different scenarios that demonstrate and validate the robustness of the proposed control law.**

I. Introduction

Control of aerial vehicles is an active topic of research, with many practical applications, such as inspection and maintenance of aging infrastructures [1]. Vertical take off and landing rotorcrafts, with hover capabilities, form a class of underactuated vehicles for which trajectory tracking controllers are necessary [2], [3]. Slung load transportation by aerial vehicles forms another class of underactuated systems for which trajectory tracking control strategies are also necessary [4]. The dynamics of an under-actuated system cannot be reduced to those of decoupled double integrators, which poses specific challenges in the control design.

Quadrotors are aerial vehicles, whose popularity stems from their ability to be used in relatively small spaces, their reduced mechanical complexity, and inexpensive components [5]. While there is noteworthy research on using quadrotors to perform specific tasks [6]–[12], in this paper we focus on slung load transportation by a quadrotor. For the latter system, the quarotor and load are attached to each other by a cable, and the control challenge lies in dampening the sway of the load with respect to the quarotor.

Different control strategies have been proposed for slung loads attached to one or several UAV's by cables. Differential flatness has been explored for the purposes of control and motion planning [13], [14], while dynamic programming has also been used for trajectory planning [15], with the goal of minimizing the load swing. Adaptive controllers have been proposed which compensate for different unknown parameters [16]–[18], such as a variable center of gravity, an unknown load mass or a constant input disturbance. Vision has been used for measuring the position of the load with respect to the aerial vehicle [19], with the visual information being used to determine the pendulous mode frequency and thereby the cable length. Load lifting by multiple aerial vehicles is found in [20]–[22]. In particular, in [20], the relations in static equilibrium between three quadrotors and a load are analyzed, and in [21] a controller is designed for three of more vehicles transporting a rigid body.

In this manuscript, we propose a control law with the objective of steering the load to a desired point in the three dimensional space. Linearization around the equilibrium is used to infer exponential stability of the same equilibrium, and conditions on the gains are provided for which exponential stability is preserved, in a similar approach to [23]. The control law includes a term which provides a means for augmenting stability [24, Chapter 7], and we study the effect of the delay introduced by the attitude inner loop on the stability of the equilibrium. Finally, we also include an integral action term in the control law for compensating for battery drainage and model mismatches, such as an unknown load mass. The proposed control law may be used to find an initial guess for gains of control laws that are harder to tune but that work for a larger subset of the state space domain, such as that proposed in [18].

The remainder of this paper is structured as follows. In Section III, the model of the quadrotor-load system and the problem statement are described. In Section IV, we provide a coordinate transformation, useful for the stability analysis. In Sections V, control laws are presented which provide closed loop stability. In Section VI, we model the quadrotor attitude inner loop, and provide conditions for which stability is preserved under the previous control laws. Finally, in Section VII, we present illustrative experimental results.

II. Notation

The map $\mathcal{S} : \mathbb{R}^3 \ni \mathbf{x} \mapsto \mathcal{S}(\mathbf{x}) \in \mathbb{R}^{3\times 3}$ yields a skew-symmetric matrix and it satisfies $\mathcal{S}(\mathbf{a})\,\mathbf{b} = \mathbf{a} \times \mathbf{b}$, for any $\mathbf{a}, \mathbf{b} \in \mathbb{R}^3$. $\mathbb{S}^2 := \{\mathbf{x} \in \mathbb{R}^3 : \mathbf{x}^T\mathbf{x} = 1\}$ denotes the set of unit vectors in $\mathbb{R}^3$. The map $\Pi : \mathbb{S}^2 \ni \mathbf{x} \mapsto \Pi(\mathbf{x}) := \mathbf{I} - \mathbf{x}\mathbf{x}^T \in \mathbb{R}^{3\times 3}$ yields a matrix that represents the orthogonal projection onto the subspace perpendicular to $\mathbf{x} \in \mathbb{S}^2$. Given $A_1, \cdots, A_n \in \mathbb{R}^{m\times m}$, for some $n, m \in \mathbb{N}$, we denote $A_1 \oplus \cdots \oplus A_n \in \mathbb{R}^{nm\times nm}$ as the block diagonal matrix with block diagonal entries A_1 to A_n. Given $\bar{\sigma} > 0$, we denote $\sigma(\cdot, \bar{\sigma}) : \mathbb{R} \ni x \mapsto \sigma(x, \bar{\sigma}) := \bar{\sigma}\frac{x}{\sqrt{\bar{\sigma}^2 + x^2}} \in (-\bar{\sigma}, \bar{\sigma})$, as a saturation function bounded by $\bar{\sigma}$; and $\sigma^{-1}(\cdot, \bar{\sigma}) : (-\bar{\sigma}, \bar{\sigma}) \ni y \mapsto \sigma^{-1}(y, \bar{\sigma}) := \bar{\sigma}\frac{y}{\sqrt{\bar{\sigma}^2 - y^2}} \in \mathbb{R}$ as the inverse mapping. We denote by $\mathbf{e}_1, \cdots, \mathbf{e}_n \in \mathbb{R}^n$ the canonical basis vectors in $\mathbb{R}^n$; when clear from the context, n is omitted.

The authors are with the School of Electrical Engineering, KTH Royal Institute of Technology, SE-100 44, Stockholm, Sweden. {ppereira, dimos}@kth.se. This work was supported by the EU H2020 Research and Innovation Programme under GA No.644128 (AEROWORKS), the Swedish Research Council (VR), the Swedish Foundation for Strategic Research (SSF) and the KAW Foundation.

III. Problem Description

Consider a quadrotor vehicle and a point mass load attached to each other by a cable, as illustrated in Fig. 1. One of the cable's end-point coincides with the quadrotor's center of mass, while the other end-point coincides with the load's center of mass. When the cable is not under tension, the load behaves as a free falling (un-actuated) point mass, while the quadrotor behaves as a *standard* quadrotor. On the other hand, when the cable is under tension, it forces the distance between the quadrotor and the load to be identical to the cable length, and for as long as the cable remains under tension. As such, a taut cable *links* the quadrotor and the load, and the load is no longer un-actuated. In fact, the system quadrotor-load may be modeled as a hybrid system, with its (open-loop) vector field switching according to some function of the state and the input. Such modeling is performed in [14], where differential flatness of the system with respect to the load's position is verified, and exploited so as to plan a trajectory for the quadrotor. In this manuscript, however, the focus is on providing a closed loop control law that guarantees that the load stabilizes around a desired point.

We denote by $\mathbf{P}, \mathbf{p} : \mathbb{R}_{\geq 0} \mapsto \mathbb{R}^3$ the quadrotor's and the load's center of mass positions, respectively; by $\mathbf{V}, \mathbf{v} : \mathbb{R}_{\geq 0} \mapsto \mathbb{R}^3$ the quadrotor's and the load's center of mass velocity vectors; by $M, m > 0$ the quadrotor's and load's masses, respectively; and, finally, by $L \in \mathbb{R}_{>0}$ the cable length. Regarding the quadrotor-load system, consider

$$\mathbf{x} = (\mathbf{p}, \mathbf{v}, \mathbf{P}, \mathbf{V}) \in \Omega_x, \tag{1}$$

$$\Omega_x := \left\{\mathbf{x} \in \mathbb{R}^{12} : \|\mathbf{P} - \mathbf{p}\| = L, (\mathbf{P} - \mathbf{p})^T(\mathbf{V} - \mathbf{v}) = 0\right\}, \tag{2}$$

$$T_{\mathbf{x}}\Omega_x := \big\{(\delta\mathbf{p}, \delta\mathbf{v}, \delta\mathbf{P}, \delta\mathbf{V}) \in \mathbb{R}^{12} : (\mathbf{P} - \mathbf{p})^T(\delta\mathbf{P} - \delta\mathbf{p}) = 0,$$
$$(\delta\mathbf{P} - \delta\mathbf{p})^T(\mathbf{V} - \mathbf{v}) + (\mathbf{P} - \mathbf{p})^T(\delta\mathbf{V} - \delta\mathbf{v}) = 0\big\}. \tag{3}$$

with (1) as a decomposition of a state, with (2) as the state space, and with (3) as the tangent space to Ω_x at some $\mathbf{x} \in \Omega_x$. Given $\mathbf{u} : \mathbb{R}_{\geq 0} \mapsto \mathbb{R}^3$, the state of the quadrotor-load system $\mathbf{x} : \mathbb{R}_{\geq 0} \mapsto \Omega_x$ evolves according to

$$\dot{\mathbf{x}}(t) = \mathbf{f}_x(\mathbf{x}(t), \mathbf{u}(t)), \mathbf{x}(0) \in \Omega_x, \tag{4}$$

where $\mathbf{f}_x : \Omega_x \times \mathbb{R}^3 \ni (\mathbf{x}, \mathbf{u}) \mapsto \mathbf{f}_x(\mathbf{x}, \mathbf{u}) \in T_{\mathbf{x}}\Omega_x \subset \mathbb{R}^{12}$ is given by

$$\mathbf{f}_x(\mathbf{x}, \mathbf{u}) := \begin{bmatrix} \mathbf{v} \\ \frac{T(\mathbf{x},\mathbf{u})}{m}\mathbf{n}(\mathbf{x}) - g\mathbf{e}_3 \\ \mathbf{V} \\ \frac{\mathbf{u}}{M} - \frac{T(\mathbf{x},\mathbf{u})}{M}\mathbf{n}(\mathbf{x}) - g\mathbf{e}_3 \end{bmatrix} \tag{5}$$

$$T(\mathbf{x}, \mathbf{u}) := \frac{m}{M + m}\left(\mathbf{u}^T\mathbf{n}(\mathbf{x}) + ML\|\mathbf{V} - \mathbf{v}\|^2\right). \tag{6}$$

with $\mathbf{x}$ as in (1) and where g is the acceleration due to gravity; and with $\mathbf{n} : \Omega_x \ni \mathbf{x} \mapsto \mathbf{n}(\mathbf{x}) \in \mathbb{S}^2$ defined as

$$\mathbf{n}(\mathbf{x}) := \frac{\mathbf{P} - \mathbf{p}}{\|\mathbf{P} - \mathbf{p}\|} \overset{(2)}{=} \frac{\mathbf{P} - \mathbf{p}}{L}. \tag{7}$$

Physically, the functions in (6) and (7) relate to the tension on the cable and to the cable's unit vector, respectively (see Fig. 1). For convenience, we also denote $\Omega_x \ni \mathbf{x} \mapsto \boldsymbol{\omega}(\mathbf{x}) := \mathcal{S}(\mathbf{n}(\mathbf{x}))\, d\mathbf{n}(\mathbf{x})\mathbf{f}_x(\mathbf{x}, \cdot) \overset{(1),(5)}{=} \mathcal{S}(\mathbf{n}(\mathbf{x}))\, \frac{\mathbf{V}-\mathbf{v}}{L}$ as the cable's angular velocity.

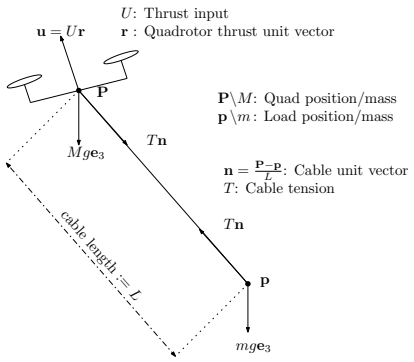

Fig. 1: Modeling of quadrotor-load system

It can be verified that indeed $\mathbf{f}_x(\mathbf{x}, \cdot) \in T_{\mathbf{x}}\Omega_x$, for any $\mathbf{x} \in \Omega_x$. In fact, for any $\mathbf{u} \in \mathbb{R}^3$, if we denote $(\delta\mathbf{p}, \delta\mathbf{v}, \delta\mathbf{P}, \delta\mathbf{V}) = \mathbf{f}_x(\mathbf{x}, \mathbf{u})$, it follows that: $(\mathbf{P} - \mathbf{p})^T(\delta\mathbf{P} - \delta\mathbf{p}) \overset{(5)}{=} (\mathbf{P} - \mathbf{p})^T(\mathbf{V} - \mathbf{v}) \overset{(2)}{=} 0$; and that $(\delta\mathbf{P} - \delta\mathbf{p})^T(\mathbf{V} - \mathbf{v}) + (\mathbf{P} - \mathbf{p})^T(\delta\mathbf{V} - \delta\mathbf{v}) \overset{(5)}{=} (\mathbf{V} - \mathbf{v})^T(\mathbf{V} - \mathbf{v}) + (\mathbf{P} - \mathbf{p})^T\left(\frac{\mathbf{u}}{M} - T(\mathbf{x}, \mathbf{u})\frac{m+M}{Mm}\mathbf{n}(\mathbf{x})\right) \overset{(7),(6),(2)}{=} 0$. As such, given the vector field in (5), it follows that a trajectory of (4) that starts in Ω_x remains in Ω_x; and, consequently, the distance between the UAV and load remains constant and equal to the cable length. We can now formulate the problem treated in this paper.

Problem 1: Given the vector field (5), design a control law $\mathbf{u}^{cl} : \Omega_x \mapsto \mathbb{R}^3$ such that $\mathbf{x}^\star = (\mathbf{p}^\star, \mathbf{v}^\star, \mathbf{P}^\star, \mathbf{V}^\star) = (\mathbf{0}, \mathbf{0}, L\mathbf{e}_3, \mathbf{0}) = L\mathbf{e}_9 \in \Omega_x \subset \mathbb{R}^{12}$ is an exponentially stable equilibrium of $\Omega_x \ni \mathbf{x} \mapsto \mathbf{f}_x^{cl}(\mathbf{x}) := \mathbf{f}_x(\mathbf{x}, \mathbf{u}^{cl}(\mathbf{x}))$.

Remark 1: Problem 1 may be reformulated so as to consider tracking of constant velocity trajectories.

IV. Coordinate Change

We wish to study the stability properties of $\mathbf{x}^\star = L\mathbf{e}_9 \in \Omega_x$ (after a control law has been chosen). However, it proves convenient to study the stability in a different coordinate system, which we associate to the letter z from now. In summary, we provide a coordinate transformation, and study the stability properties in the new coordinate system.

To start with, let us provide some useful functions. Denote, for convenience, $\Omega_\theta := (-\frac{\pi}{2}, \frac{\pi}{2}) \times (-\frac{\pi}{2}, \frac{\pi}{2})$, and $\tilde{\mathbb{S}}^2 := \mathbb{S}^2 \backslash \{\mathbf{n} \in \mathbb{S}^2 : \mathbf{e}_3^T\mathbf{n} > 0\}$. Consider the unit vector parametrization $\hat{\mathbf{n}} : \Omega_\theta \ni (\phi, \theta) =: \boldsymbol{\theta} \mapsto \hat{\mathbf{n}}(\boldsymbol{\theta}) \in \tilde{\mathbb{S}}^2$ and angle parametrization $\hat{\boldsymbol{\theta}} : \tilde{\mathbb{S}}^2 \ni \mathbf{n} \mapsto \hat{\boldsymbol{\theta}}(\mathbf{n}) \in \Omega_\theta$, defined as

$$\hat{\mathbf{n}}(\boldsymbol{\theta}) := \begin{bmatrix} \cos(\phi)\sin(\theta) \\ -\sin(\phi) \\ \cos(\phi)\cos(\theta) \end{bmatrix}, \hat{\boldsymbol{\theta}}(\mathbf{n}) := \begin{bmatrix} -\arcsin(\mathbf{e}_2^T\mathbf{n}) \\ \arctan\left(\frac{\mathbf{e}_1^T\mathbf{n}}{\mathbf{e}_3^T\mathbf{n}}\right) \end{bmatrix}. \tag{8}$$

Figure 2 illustrates geometrically the choice of angles and the mappings (8) (in essence, we associate two angles $(\phi, \theta) \in \Omega_\theta$ to the cable unit vector – see Fig. 1). We emphasize that $\hat{\mathbf{n}}(\mathbf{0}_2) = \mathbf{e}_3$, which will allow the equilibrium in the new coordinate system to be at zero; and that $\hat{\mathbf{n}}(\boldsymbol{\theta}) \circ \hat{\boldsymbol{\theta}} = \mathrm{id}_{\tilde{\mathcal{S}}^2}$ and $\hat{\boldsymbol{\theta}} \circ \hat{\mathbf{n}}(\boldsymbol{\theta}) = \mathrm{id}_{\Omega_\theta}$. Consider also $\hat{\boldsymbol{\omega}} : \Omega_\theta \times \mathbb{R}^2 \ni ((\phi, \theta), (\omega_\phi, \omega_\theta)) =: (\boldsymbol{\theta}, \boldsymbol{\omega}_\theta) \mapsto \hat{\boldsymbol{\omega}}(\boldsymbol{\theta}, \boldsymbol{\omega}_\theta) \in \mathbb{R}^3$, defined as

$$\hat{\boldsymbol{\omega}}(\boldsymbol{\theta}, \boldsymbol{\omega}_\theta) := \begin{bmatrix} -\sin(\phi)\sin(\theta) & \cos(\phi)\cos(\theta) \\ -\cos(\phi) & 0 \\ -\sin(\phi)\cos(\theta) & -\cos(\phi)\sin(\theta) \end{bmatrix} \begin{bmatrix} \omega_\phi \\ \omega_\theta \end{bmatrix}, \tag{9}$$

where $\boldsymbol{\omega}_\theta$ is interpreted as the time derivative of $\boldsymbol{\theta}$. Consider also $\boldsymbol{\omega}_{\hat{\theta}} : \tilde{\mathbb{S}}^2 \times \mathbb{R}^3 \ni (\mathbf{n}, \boldsymbol{\omega}) \mapsto \boldsymbol{\omega}_{\hat{\theta}}(\mathbf{n}, \boldsymbol{\omega}) \in \mathbb{R}^2$, defined as

$$\boldsymbol{\omega}_{\hat{\theta}}(\mathbf{n}, \boldsymbol{\omega}) := \begin{bmatrix} 0 & \frac{-1}{\sqrt{1-(\mathbf{e}_2^T\mathbf{n})^2}} & 0 \\ \frac{(\mathbf{e}_3^T\mathbf{n})}{1-(\mathbf{e}_2^T\mathbf{n})^2} & 0 & \frac{-(\mathbf{e}_1^T\mathbf{n})}{1-(\mathbf{e}_2^T\mathbf{n})^2} \end{bmatrix} \mathcal{S}(\boldsymbol{\omega})\,\mathbf{n}, \quad (10)$$

We are now in position to provide the mapping between coordinates. Denote

$$\mathbf{z} = (\mathbf{p}, \mathbf{v}, \boldsymbol{\theta}, \boldsymbol{\omega}_\theta) = ((p_x, p_y, p_z), (v_x, v_y, v_z), (\phi, \theta), (\omega_\phi, \omega_\theta)) \in \Omega_z, \quad (11)$$
$$\Omega_z = \mathbb{R}^3 \times \mathbb{R}^3 \times \Omega_\theta \times \mathbb{R}^2,$$

and consider the mappings $g_x^z : \Omega_x \ni \mathbf{x} \mapsto g_x^z(\mathbf{x}) \in \Omega_z$ and $g_z^x : \Omega_z \ni \mathbf{z} \mapsto g_z^x(\mathbf{z}) \in \Omega_x$ defined as

$$g_x^z(\mathbf{x}) := \begin{bmatrix} \mathbf{p} \\ \mathbf{v} \\ \hat{\boldsymbol{\theta}}(\mathbf{n}(\mathbf{x})) \\ \boldsymbol{\omega}_{\hat{\theta}}(\mathbf{n}(\mathbf{x}), \boldsymbol{\omega}(\mathbf{x})) \end{bmatrix}, g_z^x(\mathbf{z}) := \begin{bmatrix} \mathbf{p} \\ \mathbf{v} \\ \mathbf{p} + L\hat{\mathbf{n}}(\boldsymbol{\theta}) \\ \mathbf{v} + L\mathcal{S}(\hat{\boldsymbol{\omega}}(\boldsymbol{\theta}, \boldsymbol{\omega}_{\boldsymbol{\theta}}))\,\hat{\mathbf{n}}(\boldsymbol{\theta}) \end{bmatrix}, \quad (12)$$

with $\mathbf{x}$ as in (1) and with $\hat{\boldsymbol{\theta}}$ and $\boldsymbol{\omega}_{\hat{\theta}}$ as defined in (8) and (10); and with $\mathbf{z}$ as in (11) and with $\hat{\mathbf{n}}$ and $\hat{\boldsymbol{\omega}}$ as defined in (8) and (9). Notice that $g_x^z \circ g_z^x = \mathrm{id}_{\Omega_z}$ and that $g_z^x \circ g_x^z = \mathrm{id}_{\Omega_x}$, i.e., the mappings in (12) are inverses of each other. Notice also that $g_x^z(\mathbf{x}^\star) = \mathbf{0} \Leftrightarrow g_z^x(\mathbf{0}) = \mathbf{x}^\star$, and thus in the new coordinate system $\mathbf{z}^\star := \mathbf{0} \in \mathbb{R}^{10}$ is the equilibrium we wish to render exponentially stable (see Problem 1).

The open loop vector field in the new coordinate system, $\mathbf{f}_z : \Omega_z \times \mathbb{R}^3 \ni (\mathbf{z}, \mathbf{u}) \mapsto \mathbf{f}_z(\mathbf{z}, \mathbf{u}) \in \mathbb{R}^{10}$, is given by

$$\mathbf{f}_z(\mathbf{z}, \mathbf{u}) := dg_x^z(\mathbf{x})\mathbf{f}_x(\mathbf{x}, \mathbf{u})|_{\mathbf{x}=g_z^x(\mathbf{z})}.$$

In the new coordinates, it follows that $\mathbf{f}_z(\mathbf{0}_{10}, (M+m)g\mathbf{e}_3) = \mathbf{0}_{10}$, which means (as shall be seen later) that $\mathbf{z}^\star := \mathbf{0}_{10}$ is an equilibrium point for the closed loop vector field (intuition suggests that the equilibrium control input is $(M+m)g\mathbf{e}_3$, which corresponds to the total weight that needs to be canceled).

V. Simple Control Law

We are now in position to present the control law. For convenience, we use three subscripts, namely x, y and z, with $k \in \{x, y, z\}$ standing for the motion in the k-direction. For each $k \in \{x, y, z\}$, consider then $u_k : \mathbb{R}^2 \ni (p, v) \mapsto u_k(p, v) \in \mathbb{R}$, defined as

$$u_k(p, v) := -k_{p,k}\sigma(p, \sigma_{p,k}) - k_{v,k}\sigma(v, \sigma_{v,k}), \quad (13)$$

where σ is a saturation function (see Notation); $k_{p,k}$ and $k_{v,k}$ are positive gains related to the position and velocity feedback, respectively; and $\sigma_{p,k}$ and $\sigma_{v,k}$ are saturations related to the position and velocity feedback, respectively (note that $\sup_{(p,v)\in\mathbb{R}^2} |u_k(p, v)| = k_{p,k}\sigma_p + k_{v,k}\sigma_v$).

Consider then the control law $\mathbf{u}^{cl} : \Omega_x \ni \mathbf{x} \mapsto \mathbf{u}^{cl}(\mathbf{x}) \in \mathbb{R}^3$ defined as

$$\mathbf{u}^{cl}(\mathbf{x}) := \begin{bmatrix} M(u_x(\mathbf{e}_1^T\mathbf{P}, \mathbf{e}_1^T\mathbf{V}) + Lk_\theta\mathbf{e}_1^T\mathbf{n}(\mathbf{x})) \\ M(u_y(\mathbf{e}_2^T\mathbf{P}, \mathbf{e}_2^T\mathbf{V}) + Lk_\theta\mathbf{e}_2^T\mathbf{n}(\mathbf{x})) \\ (M+m)(g + u_z(\mathbf{e}_3^T\mathbf{p}, \mathbf{e}_3^T\mathbf{v})) \end{bmatrix}, \quad (14)$$

with u_x, u_y and u_z defined in (13) for $k \in \{x, y, z\}$. In order to compensate for model uncertainties (see Remark 2), we also make use of an integrator of the vertical load's position, which we denote by ξ (i.e., $\dot{\xi} = \mathbf{e}_3^T\mathbf{p}$). Denote then, for some $\xi \in \mathbb{R}$,

$$\mathbf{u}_\xi^{cl}(\mathbf{x}) := \mathbf{u}^{cl}(\mathbf{x}) + \mathbf{e}_3(M+m)\sigma(k_{i,z}\xi, \sigma_{i,z}). \quad (15)$$

Given the control law (15), the closed loop vector field becomes

$$\begin{bmatrix} \dot{\mathbf{z}} \\ \dot{\xi} \end{bmatrix} \equiv \mathbf{f}_z^{cl}((\mathbf{z}, \xi)) := \begin{bmatrix} \mathbf{f}_z(\mathbf{z}, \mathbf{u}_\xi^{cl}(\mathbf{x})) \\ \mathbf{e}_3^T\mathbf{p} \end{bmatrix}|_{\mathbf{x}=g_z^x(\mathbf{z})}, \quad (16)$$

with $(\mathbf{z}^\star, \xi^\star) = \mathbf{0}_{11}$ as an equilibrium of (16) (since $\mathbf{u}_0^{cl}(\mathbf{x}^\star) = (M+m)g\mathbf{e}_3$). Linearizing (16) around $\mathbf{0}_{11}$, yields the jacobian $A = d\mathbf{f}_z^{cl}(\mathbf{0}_{11}) \in \mathbb{R}^{11\times11}$, which can be transformed into a block diagonal (A is not a block diagonal matrix) via an appropriate similarity transformation. Indeed, for $P = [P_x\, P_y\, P_z]^T \in \mathbb{R}^{11\times11}$, with $P_x = [A^0\mathbf{e}_1 \cdots A^3\mathbf{e}_1] \in \mathbb{R}^{11\times4}$, $P_y = [A^0\mathbf{e}_2 \cdots A^3\mathbf{e}_2] \in \mathbb{R}^{11\times4}$, and $P_z = [\mathbf{e}_{11}\, A^0\mathbf{e}_3\, A^1\mathbf{e}_3] \in \mathbb{R}^{11\times3}$, it follows that $PAP^{-1} = A_x \oplus A_y \oplus A_z$ (see Notation), where

$$A_z = \begin{bmatrix} 0 & 1 & 0 \\ 0 & 0 & 1 \\ -k_{i,z} & -k_{p,z} & -k_{p,z} \end{bmatrix}. \quad (17)$$

and, for $h \in \{x, y\}$,

$$A_h = \begin{bmatrix} 0 & 1 & 0 & 0 \\ 0 & 0 & 1 & 0 \\ 0 & 0 & 0 & 1 \\ -\frac{g}{L}k_{p,h} & -\frac{g}{L}k_{v,h} & -(k_{p,h} + k_\theta + \frac{g}{L}\frac{M+m}{M}) & -k_{v,h} \end{bmatrix} \quad (18)$$

We have thus one chain of three integrators, related to the z motion of the load; and two chains of four integrators, related to the horizontal motion of the load; i.e., the linearized motion of the load satisfies

$$p_h^{(4)}(t) = a_{h,0}p_h^{(0)}(t) + \cdots + a_{h,3}p_h^{(3)}(t), h \in \{x, y\},$$
$$p_z^{(3)}(t) = a_{z,0}p_z^{(0)}(t) + \cdots + a_{z,2}p_z^{(2)}(t),$$

where $a_{h,i} = \mathbf{e}_4^T A_h \mathbf{e}_{i+1}$ for $i \in \{0, 1, 2, 3\}$ and $a_{z,i} = \mathbf{e}_4^T A_z \mathbf{e}_{i+1}$ for $i \in \{0, 1, 2\}$. For the roots of the characteristic polynomial of (17) to have negative real part, it suffices that $k_{i,z} < k_{p,z}k_{v,z}$ (Routh's criterion). For finding the location of the roots of the characteristic polynomial of (18) w.r.t. the imaginary axis, we apply the Routh's criterion to (18) [24, Chapter 7], and obtain (these are the numbers in the first column of the Routh's table)

$$\begin{bmatrix} 1 & k_{v,h} & k_{v,h}\left(\frac{g}{L}\frac{m}{M} + k_\theta + k_{p,h}\right) & \frac{g}{L}\left(\frac{g}{L}\frac{m}{M} + k_\theta\right)k_{v,h}^2 & \frac{g}{L}k_{p,h} \end{bmatrix}, \quad (19)$$

which guarantees exponential stability of the equilibrium $(\mathbf{z}^\star, \xi^\star) = \mathbf{0}_{11}$ of (16), provided that $k_\theta > -\left(\frac{g}{L}\frac{m}{M} + k_{p,h}\right)$ for $h \in \{x, y\}$, since in that case all entries in (19) are positive (recall that $k_{p,h} > 0$ and $k_{v,h} > 0$). Notice that exponential stability is guaranteed if $k_\theta = 0$; however, including the gain k_θ in the control law (14) provides a

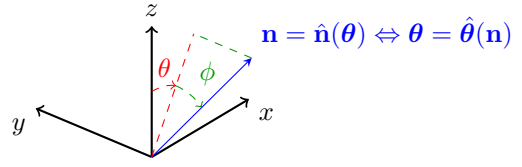

Fig. 2: Geometic interpretation of (8) for $\mathbf{n} \in \tilde{\mathbb{S}}^2$ and $\boldsymbol{\theta} = (\phi, \theta) \in \Omega_\theta$

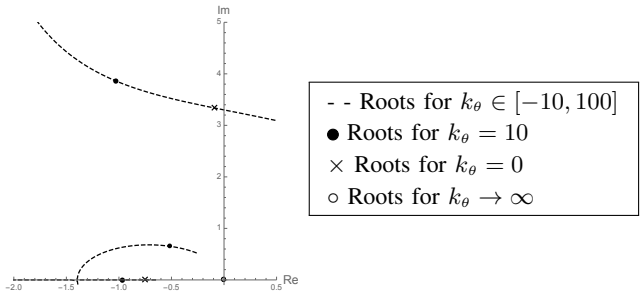

Fig. 3: Roots of characteristic polynomial of A_x, in (18), in complex plane (conjugate poles are omitted); all other constants are those provided in Section VII.

means of augmenting stability [24, Chapter 7], i.e., of placing the roots of the characteristic polynomial of the linearization matrix in better locations, in the sense that they lead to a better transient response (faster convergence and/or fewer oscillations). More importantly, we can look at the roots of the characteristic polynomial of (18) for different values of k_θ, as done in Fig. 3. As can be seen, increasing k_θ (for example, from 0 to 10 see Fig. 3) has the benefit of making the system faster, i.e., of increasing the speed of convergence to the equilibrium. As such, k_θ can be tuned so as to augment the stability of the closed loop.

Remark 2: If the load's mass is unknown, and the control law (15) is implemented with $m = 0$, the equilibrium becomes $(\mathbf{x}^\star, \xi^\star) = \left(L\mathbf{e}_9, \sigma^{-1}(\frac{g}{k_{i,z}}\frac{m}{M+m}, \sigma_{i,z})\right)$ (well defined if $mg < (M+m)k_{i,z}\sigma_{i,z}$), since $\mathbf{u}^{cl}_{\xi^\star}(\mathbf{x}^\star) = (M+m)g$, which corresponds to the combined weight of the UAV and load necessary for maintenance of the equilibrium. As such, for an unknown mass, the steady state integral action can compensate for the model mismatch.

VI. Attitude Control Inner Loop

Previously, in Section III, we assumed that the UAV provides the requested input without delay. However, that is not the case in a real physical system, and it is important to study the effect of the attitude inner loop dynamics in the closed loop stability for the proposed control law. From here on, we work with augmented states and use a bar notation to denote those. Consider then the augmented state,

$$\bar{\mathbf{x}} = (\mathbf{x}, \mathbf{r}) \in \Omega_x \times \mathbb{S}^2 =: \Omega_{\bar{x}} \tag{20}$$

where $\mathbf{r} \in \mathbb{S}^2$ is the quadrotor's direction where input thrust is provided (see Fig. 1). The state $\bar{\mathbf{x}} : \mathbb{R}_{\geq 0} \mapsto \Omega_{\bar{x}}$ evolves according to

$$\dot{\bar{\mathbf{x}}}(t) = \mathbf{f}_{\bar{x}}(\bar{\mathbf{x}}(t), \mathbf{u}(t)), \bar{\mathbf{x}}(0) \in \Omega_{\bar{x}}$$

where $\mathbf{f}_{\bar{x}} : \Omega_{\bar{x}} \times (\mathbb{R}^3 \backslash \{\mathbf{0}\}) \ni (\bar{\mathbf{x}}, \mathbf{u}) \mapsto \mathbf{f}_{\bar{x}}(\bar{\mathbf{x}}, \mathbf{u}) \in T_{\bar{\mathbf{x}}}\Omega_{\bar{x}} \subset \mathbb{R}^{15}$ is given by

$$\mathbf{f}_{\bar{x}}(\bar{\mathbf{x}}, \mathbf{u}) := \begin{bmatrix} \mathbf{f}_x(\mathbf{x}, \mathbf{u}^T\mathbf{r}\mathbf{r}) \\ \mathbf{f}_r(\mathbf{r}, \mathbf{u}) \end{bmatrix} := \begin{bmatrix} \mathbf{f}_x(\mathbf{x}, \mathbf{u}^T\mathbf{r}\mathbf{r}) \\ k_{\bar{\theta}}\Pi(\mathbf{r})\frac{\mathbf{u}}{\|\mathbf{u}\|} \end{bmatrix}, \tag{21}$$

with $\mathbf{f}_x$ as in (5), and with $k_{\bar{\theta}}$ as a positive gain that relates to the fastness of the attitude inner loop ($\frac{1}{k_{\bar{\theta}}}$ may be interpreted as a time constant of a first order system).

Let us provide some intuition for (21). Consider a constant $\mathbf{r}^\star \in \mathbb{S}^2$ and the function $V : \mathbb{S}^2 \ni \mathbf{r} \mapsto V(\mathbf{r}) := 1 - \mathbf{r}^T\mathbf{r}^\star \in [0, 2]$. Then, along solutions of $\dot{\mathbf{r}}(t) = \mathbf{f}_r(\mathbf{r}(t), \mathbf{r}^\star)$, it follows that $\dot{V}(\mathbf{r}(t)) = -k_{\bar{\theta}}V(\mathbf{r}(t))(2 - V(\mathbf{r}(t)))$; this suffices to conclude that $t \mapsto V(\mathbf{r}(t))$ converges to either 0 or 2. In fact, it converges to 0 as long as $\mathbf{r}(0) \neq -\mathbf{r}^\star$, and it converges exponential fast. Thus, loosely speaking, if $k_{\bar{\theta}}$ is *big* and $t \mapsto \mathbf{u}(t)$ is slow varying, $t \mapsto \mathbf{r}(t) - \frac{\mathbf{u}(t)}{\|\mathbf{u}(t)\|}$ converges exponentially fast to $\mathbf{0}$; this in turn guarantees that $t \mapsto \mathbf{u}^T(t)\mathbf{r}(t)\mathbf{r}(t) - \mathbf{u}(t)$ converges to $\mathbf{0}$, in which case the model in Section III is recovered. Note that $\mathbf{f}_r$ models the attitude inner loop of the quadrotor in (21), but there are more ways of modeling that inner loop.

As done in Section IV, it is convenient to work in a new coordinate system. For that reason, denote

$$\bar{\mathbf{z}} = (\mathbf{z}, \bar{\boldsymbol{\theta}}) = (\mathbf{z}, (\bar{\phi}, \bar{\theta})) \in \Omega_{\bar{z}} \overset{\mathbf{z} \text{ as in (11)}}{=} \Omega_z \times \Omega_\theta, \tag{22}$$

and consider $g^{\bar{z}}_{\bar{x}} : \Omega_{\bar{x}} \ni \bar{\mathbf{x}} \mapsto g^{\bar{z}}_{\bar{x}}(\bar{\mathbf{x}}) \in \Omega_{\bar{z}}$ and $g^{\bar{x}}_{\bar{z}} : \Omega_{\bar{z}} \ni \bar{\mathbf{z}} \mapsto g^{\bar{x}}_{\bar{z}}(\bar{\mathbf{z}}) \in \Omega_{\bar{x}}$ defined as

$$g^{\bar{z}}_{\bar{x}}(\bar{\mathbf{x}}) := \begin{bmatrix} g^z_{\bar{x}}(\mathbf{x}) \\ \hat{\boldsymbol{\theta}}(\mathbf{r}) \end{bmatrix}, g^{\bar{x}}_{\bar{z}}(\bar{\mathbf{z}}) := \begin{bmatrix} g^x_z(\mathbf{z}) \\ \hat{\mathbf{n}}(\bar{\boldsymbol{\theta}}) \end{bmatrix}, \tag{23}$$

with $\bar{\mathbf{x}}$ and $\bar{\mathbf{z}}$ as in (20) and (22); and with $\hat{\boldsymbol{\theta}}$ and $\hat{\mathbf{n}}$ as in (8). Geometrically, we parametrize the quadrotor unit vector $\mathbf{r}$ (see Fig. 1) by two angles $\bar{\boldsymbol{\theta}} = (\bar{\phi}, \bar{\theta}) \in \Omega_\theta$ similarly to the parametrization of the cable unit vector $\mathbf{n}$ by $\boldsymbol{\theta} = (\phi, \theta) \in \Omega_\theta$ (see Fig. 2). From (23), one can construct the open loop vector field for the augmented system, $\mathbf{f}_{\bar{z}}(\bar{\mathbf{z}}, \mathbf{u}) \overset{(22)}{:=} dg^{\bar{z}}_{\bar{x}}(\bar{\mathbf{x}})\mathbf{f}_{\bar{x}}(\bar{\mathbf{x}}, \mathbf{u})|_{\bar{\mathbf{x}}=g^{\bar{x}}_{\bar{z}}(\bar{\mathbf{z}})}$, for which it holds that $\mathbf{f}_{\bar{z}}(\mathbf{0}_{12}, (M+m)g\mathbf{e}_3) = \mathbf{0}_{12}$ (and thus $\mathbf{0}_{12}$ is an equilibrium).

Consider then the control law (15), which leads to the closed loop vector field $(\dot{\bar{\mathbf{z}}}, \dot{\xi}) \equiv \mathbf{f}^{cl}_{\bar{z}}((\bar{\mathbf{z}}, \xi)) = (\mathbf{f}_{\bar{z}}(\bar{\mathbf{z}}, \mathbf{u}^{cl}_\xi(\mathbf{x})), \mathbf{e}_3^T\mathbf{p})|_{\mathbf{x}=g^x_z(\mathbf{z})}$ and to the jacobian matrix $\bar{A} = d\mathbf{f}^{cl}_{\bar{z}}(\mathbf{0}_{13})$. Similarly to as in Section V, consider the similarity matrix $\bar{P} = [\bar{P}_x\, \bar{P}_y\, \bar{P}_z]^T \in \mathbb{R}^{13\times 13}$ with $\bar{P}_x = \left[\bar{A}^0\mathbf{e}_1 \cdots \bar{A}^4\mathbf{e}_1\right] \in \mathbb{R}^{13\times 5}$, $\bar{P}_y = \left[\bar{A}^0\mathbf{e}_2 \cdots \bar{A}^4\mathbf{e}_2\right] \in \mathbb{R}^{13\times 5}$, and $\bar{P}_z = \left[\mathbf{e}_{13}\, \bar{A}^0\mathbf{e}_3\, \bar{A}^1\mathbf{e}_3\right] \in \mathbb{R}^{13\times 3}$, for which it follows that $\bar{P}\bar{A}\bar{P}^{-1} = \bar{A}_x \oplus \bar{A}_y \oplus \bar{A}_z$, where $\bar{A}_z = A_z$ (see (17)) and, for $h \in \{x, y\}$,

$$\bar{A}_h = \left[\begin{array}{cccc|c} \multicolumn{4}{c|}{\begin{bmatrix} 0 & 1 & 0 & 0 \\ 0 & 0 & 1 & 0 \\ 0 & 0 & 0 & 1 \\ 0 & 0 & 0 & 0 \end{bmatrix}} & \begin{bmatrix} 0 \\ 0 \\ 0 \\ 1 \end{bmatrix} \\ \hline \multicolumn{4}{c|}{-k_{\bar{\theta}}\mathbf{e}_4^T A_h^2 - \frac{g}{L}\frac{M+m}{M}\mathbf{e}_4^T} & -k_{\bar{\theta}} \end{array}\right]. \tag{24}$$

As such, when considering the system (21) with an attitude inner loop, we have one chain of three integrators, related to the z motion of the load (as in Section V); and two chains of five integrators, related to the horizontal motion of the load (as opposed to four, as in Section V). For finding the location of the roots of the characteristic polynomial of (24) w.r.t. the imaginary axis, we apply the Routh's criterion, and obtain, by setting $k_\theta = 0$ (for convenience, denote $\gamma = k_{\bar{\theta}}k_{v,h} - k_{p,h}$)

$$\begin{bmatrix} 1 & k_{\bar{\theta}} & k_{\bar{\theta}}\gamma & k^2_{\bar{\theta}}\gamma\left(\frac{g}{L}\frac{m}{M} + k_{p,h}\right) & k^2_{\bar{\theta}}\frac{g^2}{L^2}\frac{m}{M}\gamma^2 & \frac{g}{L}k_{p,h} \end{bmatrix}. \tag{25}$$

Thus exponential stability of the equilibrium is preserved for as long as $\gamma > 0 \Leftrightarrow k_{\bar{\theta}} > \frac{k_{p,h}}{k_{v,h}}$, i.e., provided that the attitude gain is *big enough*. Since, we do not have control over $k_{\bar{\theta}}$, preserving stability amounts to guaranteeing that $\frac{k_{p,h}}{k_{v,h}}$, for

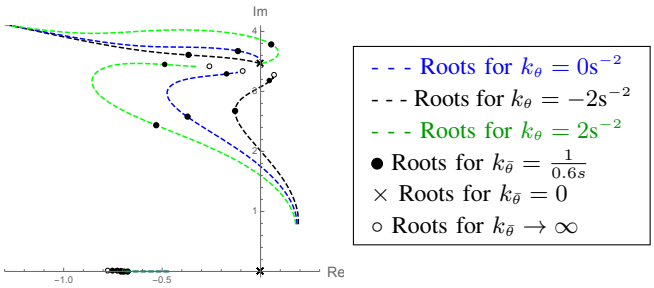

Fig. 4: Roots of characteristic polynomial of $\bar{A}_x$, in (24), in complex plane, for $k_{\bar\theta} \in [0.1, 10]\text{s}^{-1}$ (conjugate poles are omitted); all other constants are those in Section VII.

$h \in \{x, y\}$, remains *small enough*.

Theorem 3: Consider the quadrotor-load system with the open loop vector field (21), and the control law (14) with $k_\theta = 0$. Then, the equilibrium $\bar{\mathbf{x}}^\star = (L\mathbf{e}_9, \mathbf{e}_3) \in \Omega_{\bar x} \times \mathbb{S}^2$ of $\Omega_{\bar x} \ni \bar{\mathbf{x}} \mapsto \mathbf{f}^{cl}_{\bar x}(\bar{\mathbf{x}}) \overset{(20)}{:=} \mathbf{f}_{\bar x}(\bar{\mathbf{x}}, \mathbf{u}^{cl}(\mathbf{x}))$ is exponentially stable iff $k_{\bar\theta} > \max\limits_{h\in\{x,y\}} \frac{k_{p,h}}{k_{v,h}}$, i.e., iff the attitude inner loop is sufficiently fast.

Proof: Linearizing $\mathbf{f}^{cl}_{\bar z}(\bar{\mathbf{z}}) := dg^{\bar z}_{\bar x}(\bar{\mathbf{x}})\mathbf{f}^{cl}_{\bar x}(\bar{\mathbf{x}})|_{\bar{\mathbf{x}}=g^{\bar x}_{\bar z}(\bar{\mathbf{z}})}$ around $\bar{\mathbf{z}}^\star = g^{\bar z}_{\bar x}(\bar{\mathbf{x}}^\star) = \mathbf{0}$ yields the matrix (24) with $k_\theta = 0$. Exponential stability of the equilibrium follows from the Routh's criterion through equation (25). ■

If we apply the Routh's criterion for arbitrary k_θ, we obtain

$$\begin{bmatrix} 1 & k_{\bar\theta} & k_{\bar\theta}(k_{\bar\theta}k_{v,h} - (k_{p,h} + k_\theta)) & \gamma_1 & \gamma_2 & \frac{g}{L}k_{p,h} \end{bmatrix}, \quad (26)$$

where γ_1 and γ_2 are quadratic expressions on k_θ and $k_{\bar\theta}$, which we omit for brevity. Thus the equilibrium is exponentially stable only if (the condition below is necessary, but not sufficient: for sufficiency, positiveness of all entries in (26) must be guaranteed.)

$$k_{\bar\theta} > (k_{p,h} + k_\theta)/k_{v,h} \Leftrightarrow k_\theta < k_{\bar\theta}k_{v,h} - k_{p,h}. \quad (27)$$

In Section V, it was deduced that choosing a positive k_θ augmented the closed loop stability; however, notice from (27) that a larger k_θ requires a larger $k_{\bar\theta}$, and, consequently, for a *slow* attitude inner loop (where $k_{\bar\theta}$ is *small*), choosing a *large* positive k_θ, instead of augmenting stability, may actually render the equilibrium unstable.

In Fig. 4, the roots are plotted for different k_θ and for $k_{\bar\theta} \in \left[\frac{1}{10}, 10\right]\text{s}^{-1}$. As can be seen, choosing a positive k_θ may actually render the equilibrium unstable (see Fig. 4 with $k_\theta = 2\text{s}^{-2}$). As expected, notice that the equilibrium becomes unstable when $k_{\bar\theta} \to 0$, i.e., when the attitude inner loop becomes *too slow*. In fact, for each $k_{\bar\theta} > 0$ there is an interval for k_θ where exponential stability is preserved.

VII. Experimental Results

For the experiments, a commercial quadrotor was used, namely an IRIS+ from 3D Robotics, weighting $M = 1.442$ kg, with a maximum payload of 0.4 kg. For the load, a wood block weighting $m = 0.145$ kg (corresponding to $\approx 10\%$ of the UAV's weight) was chosen, attached to the UAV by a cable of $L = 0.9$ m. The commands for controlling the quadrotor are processed on a ground station, developed in a ROS environment, and sent to the on-board autopilot, which allows for remotely controlling the aerial vehicle through a desired three dimensional force input. A wireless radio communication between ground station and autopilot is established through a telemetry radio, using a MAVLink protocol that directly overrides the signals sent from the radio transmitter. The quadrotor's and load's position and velocity are estimated by 12 cameras from a Qualisys motion capture system.

The control law (15) is applied, with $k_{i,z} = 0.25\text{s}^{-3}$ and $\sigma_{i,z} = 0.5\text{ms}^{-2}$; with $k_\theta = -2\text{s}^{-2}$; with $k_{p,x} = k_{p,y} = 3.5\text{s}^{-2}$, $k_{v,x} = k_{v,y} = 5.5\text{s}^{-1}$, $\sigma_{p,x} = \sigma_{p,y} = 0.5$m and $\sigma_{v,x} = \sigma_{v,y} = 0.5\text{ms}^{-1}$; with $k_{p,z} = 1.0\text{s}^{-2}$, $k_{v,z} = 1.2\text{s}^{-1}$, $\sigma_{p,z} = 0.5$m and $\sigma_{v,z} = 0.5\text{ms}^{-1}$ (see (14)). We provide three experiments displayed in the companion video submitted with the paper, and figures for two of those experiments in Figs. 5–6.

In Fig 5, the load is required to hover at $0.5\mathbf{e}_3$m, and the control law is tested for robustness with respect to disturbances; first, the load is disturbed in the x-direction (at $t \approx 8$s); then disturbed in the y-direction (at $t \approx 18$s); and, finally, the UAV is disturbed in the x-direction (at $t \approx 28$s). The effect of these disturbances is seen in all Figs. 5(a)–5(d). All these disturbances are well damped, as seen in Fig. 5(c). In Fig 6, the load is required to hover at the consecutive points in $\{[0\ 0\ 0.5], [1.2\ 1.2\ 0.5], [1.2\ -1.2\ 0.5], [-1.2\ -1.2\ 0.5], [-1.2\ 1.2\ 0.5], [0\ 0\ 0.5]\}$m. There is an interval of ten seconds between consecutive points, which correspond to the corners of a square (see Fig. 6(a)). The tracking performance is shown in Fig. 6(b), and the larger standard deviation of the cable angles is around $3.2°$ – see Fig. 6(c). An extra experiment, where the load is required to describe a circle, is shown in the companion video but figures showing the tracking performance and cable sway are omitted due to space constraints.

In Fig .7(b), the actual input requested to the IRIS vehicle is presented for the first experiment, the one in Fig. 5. It is comprised of three PWM signals (we omit the signal for the yaw channel): one for the pitch, one for the roll, and another for the throttle. The pitch and roll PWM signals have neutral values for which the quadrotor does not pitch nor roll, regardless of battery level; while the throttle PWM signal results in a propulsive power which decays as the battery drains. Figure 7(a) shows the integral action for all three experiments. There is a trend, where the integral term grows larger while the experiments are running, which stems from the fact that, as the batteries drain, a larger throttle PWM signal needs to be requested from the IRIS+.

VIII. Conclusions

We proposed a control law for stabilization of a quadrotor-load system, and provided conditions on the control law's gains that guarantee exponential stability of the equilibrium. The UAV was modeled with an attitude inner loop, and a lower bound on the attitude gain for which exponential stability of the equilibrium is preserved was provided. Finally, we also included an integral action term in the control law so as to compensate for battery drainage or model mismatches, such as an unknown load mass. Experiments for different scenarios demonstrate and validate the robustness of the proposed control law.

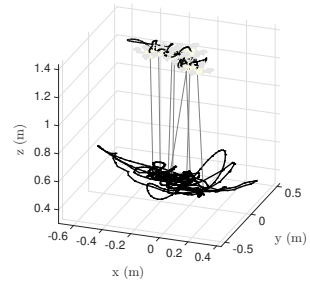

(a) Trajectory of system UAV+load

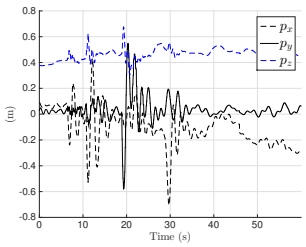

(b) Load position

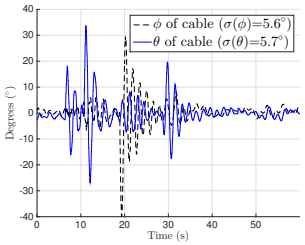

(c) Cable angles (see (8) and (7))

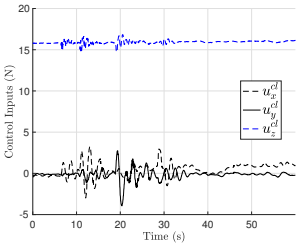

(d) Control input, $\mathbf{u}_\xi^{cl}$ (see (15))

Fig. 5: Impulse disturbances on UAV+load system (disturbance on load in the x and y directions, at $t \approx 8$s and $t \approx 18$s; disturbance on UAV in the x-direction, at $t \approx 27$s).

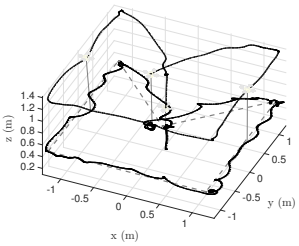

(a) Trajectory of system UAV+load

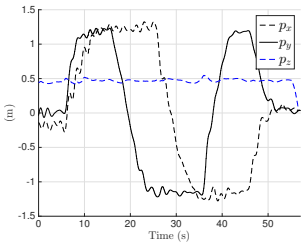

(b) Load position

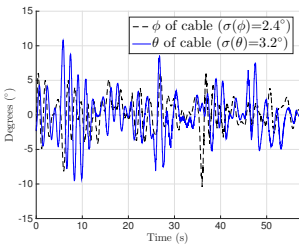

(c) Cable angles (see (8) and (7))

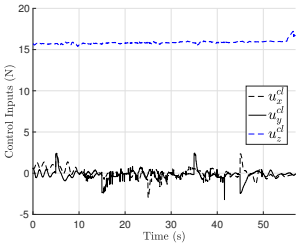

(d) Control input $\mathbf{u}_\xi^{cl}$ (see (15))

Fig. 6: System UAV+load, with load required to move to the corners of a square of length 1.2m, at intervals of 10s.

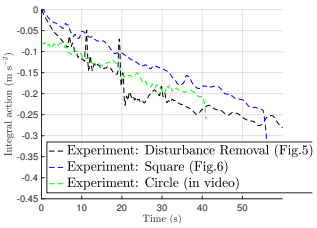

(a) Integral action $\sigma(k_{i,z}\xi, \sigma_{i,z})$ in (15), for all three experiments.

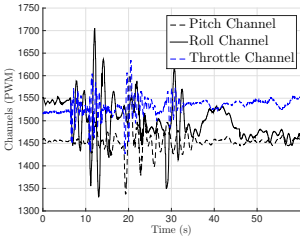

(b) Control input $\mathbf{u}_\xi^{cl}$ converted to PWM sent to the IRIS+, for the experiment in Fig. 5.

Fig. 7: Integral action and IRIS+ PWM signals

References

[1] AEROWORKS aim. http://www.aeroworks2020.eu/.

[2] M. Hua, T. Hamel, P. Morin, and C. Samson. Introduction to feedback control of underactuated vtol vehicles: A review of basic control design ideas and principles. *Control Systems*, 33(1):61–75, 2013.

[3] M. Bangura and R. Mahony. Real-time model predictive control for quadrotors. *IFAC Proceedings Volumes*, 47(3):11773 – 11780, 2014. 19th IFAC World Congress.

[4] M. Bernard and K. Kondak. Generic slung load transportation system using small size helicopters. In *IEEE International Conference on Robotics and Automation*, pages 3258–3264. IEEE, 2009.

[5] R. Mahony, V. Kumar, and P. Corke. Multirotor aerial vehicles: Modeling, estimation, and control of quadrotor. *Robotics Automation Magazine, IEEE*, 19(3):20–32, Sept 2012.

[6] F. Ruggiero et al. A multilayer control for multirotor uavs equipped with a servo robot arm. In *IEEE International Conference on Robotics and Automation*, pages 4014–4020, 2015.

[7] M. Tognon and A. Franchi. Nonlinear observer-based tracking control of link stress and elevation for a tethered aerial robot using inertial-only measurements. In *IEEE International Conference on Robotics and Automation*, pages 3994–3999, 2015.

[8] D. Scaramuzza and et al. Vision-controlled micro flying robots: From system design to autonomous navigation and mapping in GPS-denied environments. *Robotics Automation Magazine, IEEE*, 21(3):26–40, Sept 2014.

[9] J.L.J. Scholten, M. Fumagalli, S. Stramigioli, and R. Carloni. Interaction control of an UAV endowed with a manipulator. In *IEEE International Conference on Robotics and Automation (ICRA)*, pages 4910–4915, May 2013.

[10] M Orsag, C. M. Korpela, S. Bogdan, and P. Y. Oh. Hybrid adaptive control for aerial manipulation. *Journal of Intelligent & Robotic Systems*, 73(1):693–707, 2013.

[11] M. B. Srikanth, A. Soto, A. Annaswamy, E. Lavretsky, and J.-J. Slotine. Controlled manipulation with multiple quadrotors. In *AIAA Guidance, Navigation, and Control Conference*, 8 2011.

[12] H. Lee, H. Kim, and H.J. Kim. Path planning and control of multiple aerial manipulators for a cooperative transportation. In *IEEE/RSJ International Conference on Intelligent Robots and Systems (IROS)*, pages 2386–2391, Sept 2015.

[13] É. Servais, H. Mounier, and B. d'Andréa Novel. Trajectory tracking of trirotor UAV with pendulum load. In *20th International Conference on Methods and Models in Automation and Robotics (MMAR)*, pages 517–522, Aug 2015.

[14] K. Sreenath, N. Michael, and V. Kumar. Trajectory generation and control of a quadrotor with a cable-suspended load - a differentially-flat hybrid system. In *ICRA*, pages 4888–4895. IEEE, 2013.

[15] I. Palunko, R. Fierro, and P. Cruz. Trajectory generation for swing-free maneuvers of a quadrotor with suspended payload: A dynamic programming approach. In *IEEE ICRA*, pages 2691–2697, 2012.

[16] I. Palunko, P. Cruz, and R. Fierro. Agile load transportation. *IEEE Robotics Automation Magazine*, 19(3):69–79, 9 2012.

[17] S. Dai, T. Lee, and D. S. Bernstein. Adaptive control of a quadrotor uav transporting a cable-suspended load with unknown mass. In *IEEE Conference on Decision and Control*, pages 6149–6154, 2014.

[18] P. Pereira, M. Herzog, and D. V. Dimarogonas. Slung load transportation with single aerial vehicle and disturbance removal. In *24th Med. Conf. on Control and Automation*, pages 671–676, 2016.

[19] M. Bisgaard, A. la Cour-Harbo, and J. D. Bendtsen. Adaptive control system for autonomous helicopter slung load operations. *Control Engineering Practice*, 18(7):800–811, 2010.

[20] N. Michael, J. Fink, and V. Kumar. Cooperative manipulation and transportation with aerial robots. *Autonomous Robots*, 30(1):73–86, 2011.

[21] T. Lee. Geometric control of multiple quadrotor uavs transporting a cable-suspended rigid body. In *IEEE Conference on Decision and Control*, pages 6155–6160, 2014.

[22] I. Maza, K. Kondak, M. Bernard, and A. Ollero. Multi-uav cooperation and control for load transportation and deployment. *Journal of Intelligent and Robotic Systems*, 57(1-4):417–449, 2010.

[23] P. E.I. Pounds, D.R. Bersak, and A.M. Dollar. Grasping from the air: Hovering capture and load stability. In *IEEE International Conference on Robotics and Automation*, pages 2491–2498, May 2011.

[24] R. C. Nelson. *Flight stability and automatic control*, volume 2. WCB/McGraw Hill, 1998.